Improving unsupervised graph-based skull stripping: enhancements and comparative analysis with state-of-the-art methods

Maria Popa[1,*,†], Anca Andreica[1,†]

[1]Babeş-Bolyai University, Faculty of Mathematics and Computer Science, Department of Computer Science, Mihail Kogălniceanu 1, 400084, Cluj-Napoca, Romania

Abstract

Brain disorders are increasingly prevalent today, making accurate brain segmentation essential for effective treatment and recovery. This paper introduces an enhanced unsupervised graph-based brain segmentation method that employs an ellipsoid to select the nodes forming the graph. The method was rigorously evaluated on T1 and T2 modalities using four diverse datasets: the complete NFBS dataset, 48 MRIs from the IXI dataset, 16 images featuring infant data from the QIN dataset, and 36 images from the FMS dataset. Comparative analysis with two widely used state-of-the-art approaches, BET2 and BSE, revealed that the proposed method significantly improved segmentation results. On the infant dataset, the method achieved a 21% increase in sensitivity compared to BSE, along with a 14% improvement in precision and a 13% increase in the Jaccard index compared to BET2. On the NFBS dataset, it demonstrated a 10% improvement in precision over BET2. However, on the T2-weighted dataset, only slight improvements were observed compared to both BSE and BET2. This advancement in segmentation techniques holds promise for better diagnosis and treatment of various brain disorders, potentially leading to improved patient outcomes and more efficient clinical workflows.

Keywords

Skull Stripping, Brain Extraction, Graph-Based Segmentation, Unsupervised Segmentation, BET, BSE

1. Introduction

According to the World Health Organization (WHO), approximately 38 million people are affected by Alzheimer's disease, the most prevalent form of dementia. Epilepsy, a chronic noncommunicable brain disorder, can impact individuals of all ages, with an estimated 50 million people worldwide experiencing this condition. Accurate segmentation is a crucial step in early detection and regular examinations of brain disorders, as it is essential for identifying suitable treatments and ultimately promoting healing. The extensive use of MRI, a painless and rapid diagnostic tool, is prevalent in screening. The necessity for precise computer-assisted systems arises because manual segmentation is time-consuming and imposes additional workload on the medical staff.

Accurate segmentation is a crucial step in early detection and regular examinations of brain disorders, as it is essential for identifying suitable treatments and ultimately promoting healing. The extensive use of MRI, a painless and rapid diagnostic tool, is prevalent in screening. The necessity for precise computer-assisted systems arises because manual segmentation is time-consuming and imposes additional workload on the medical staff.

Brain segmentation, also known as skull stripping, involves the process of separating the skull from the brain. While various methods have been proposed in the literature, both supervised and unsupervised, for this purpose, the absence of a universally perfect method persists due to the diverse range of systems and the multitude of brain-related issues.

The Brain Extraction Tool (BET) [1] is an unsupervised method used for skull stripping. Its widespread adoption is due to its speed and robustness. The algorithm is based on surface tessellation, approximating

IDDM'24: 7th International Conference on Informatics & Data-Driven Medicine, November 14 - 16, 2024, Birmingham, UK

*Corresponding author.

†These authors contributed equally.

maria.popa@ubbcluj.ro (M. Popa); anca.andreica@ubbcluj.ro (A. Andreica)

0009-0009-9335-5954 (M. Popa); 0000-0003-2363-5757 (A. Andreica)

the brain with a sphere, and extracting it through 1000 iterations. One drawback of the method is its inability to effectively segment the bottom and top of the brain, leading to the inclusion of non-brain tissue in the segmentation. Although BET* [2] attempts to address these issues by reducing the number of iterations to 50 and approximating the brain with an ellipsoid, it still incorporates non-brain tissue into the segmentation [3, 4].

GUBS [5] is an unsupervised graph-based segmentation method that represents MRI volumes as a weighted graph, with nodes corresponding to voxels and edges capturing relations between them. The weight for each edge is determined by calculating the absolute difference in intensity between the two nodes. Then, the algorithm classifies voxels into three categories, namely, nodes inside the brain, nodes in the non-brain tissue(skull) and nodes from the background. Subsequently, a minimal spanning tree is constructed by collapsing the entire graph to the selected nodes. The node selection process depends on the dataset and the user interaction. Analyzing the dataset is crucial for determining the threshold above which nodes are selected, as well as establishing the boundary for the skull [3].

Some recent studies [4] and [3] aim to overcome these problems by eliminating user interaction and dependency on parameters for each dataset. These methods reduce the number of node categories to just two: nodes inside the brain and nodes in the background. The node selection approach eliminates user interaction by approximating the brain with either a sphere [3] or an ellipsoid [4]. In both approaches, the center of the geometric bodies is set at the center of the mass of the image. These methods show improved results compared to the GUBS approach and halve the time needed to process one MRI. Although the method was only tested on NFBS [6] dataset and it still includes non-brain tissue into segmentation.

The paper introduces an enhanced 3D unsupervised graph-based method for brain segmentation. By addressing the limitations of Ellipsoid-GUBS [4] and maintaining zero user interaction, it achieves heightened segmentation accuracy. The method is tested across various datasets and compared to two state-of-the-art methods, demonstrating improved results. The following are the key contributions of our work:

1. **Geometric Centering:** The novelty of the proposed method lies in the shift from center-of-mass placement of the ellipsoid to a fixed geometric center within the image. This adjustment reduces sensitivity to asymmetrical or irregular mass distributions, leading to more stable segmentation outcomes across varying datasets
2. **Comprehensive Validation Across Datasets:** Another key contribution is the comprehensive evaluation of the method on four diverse datasets, showcasing its robustness and adaptability in comparison to the previous version, which was tested on a single dataset
3. **Benchmarking Against State-of-the-Art:** ncluding comparisons with two state-of-the-art methods is crucial for benchmarking and demonstrates that our approach has notable advantages. Specifically, it shows superior robustness (working effectively with T2 modality and infant data) and offers accurate segmentation.

The remaining sections of the paper are organized as follows: Section 2 provides an overview of related work, Section 3 introduces a new approach, Section 4 outlines the experiments and their results, Section 5 delves into a discussion, and Section 6 concludes with remarks on future work.

2. Related work

Graph-based applications have gained prominence in modern methodologies due to their robust capability to depict complex relationships within data. These applications find versatile utility across a range of fields, including social network analysis and biological systems modeling, where the interconnected nature of entities can be effectively represented and analyzed. The adaptability of graph structures positions them as invaluable tools for tackling intricate problems that require an understanding and utilization of complex connections among different data points. Consequently, the prevalence of graph-based approaches has grown in modern data-driven applications, underscoring their significance and effectiveness in capturing and interpreting intricate data relationships.

Graph-CUTS [7, 3] stands out as a widely adopted skull stripping method employing morphological operations for brain segmentation. In the segmentation phase, region growing is employed to estimate the white matter volume. The subsequent step involves transforming the resulting MRI into a graph and applying graph-cuts to eliminate narrow connections. One drawback of this method lies in its dependency on region growth, which may introduce a time-consuming aspect.

GUBS [5, 3], along with the methodologies introduced in [3] and [4], employs a Minimum Spanning Tree (MST) for brain segmentation. The MRI is initially translated into a graph, and subsequently, a MST is constructed by collapsing the nodes. In [3], the drawbacks of GUBS are acknowledged, and a user-friendly interaction approach is introduced, resulting in enhanced outcomes compared to GUBS. While the results are not flawless, the method demonstrates improvement by sampling nodes within an ellipsoid, as outlined in [4].

BET2 [8], an enhanced version of the BET algorithm, is part of the FSL Tool suite [9]. BET2 is optimized for high-resolution T1 and T2-weighted images and ideally requires paired T1 and T2-weighted scans with a resolution of approximately 2 mm. Initially, the brain surface is identified in the T1 image using the original BET algorithm, after which the T2 image is registered to the T1 scan [10, 11]. Compared to BET, BET2 achieves more accurate segmentation results [11].

The Brain Surface Extraction (BSE) method utilizes anisotropic diffusion to enhance brain boundaries [10, 11]. Edge detection is performed with a 2D Marr-Hildreth operator, combining low-pass filtering using a Gaussian kernel and locating zero crossings in the Laplacian of the filtered image. BSE disconnects the brain from surrounding tissues via morphological erosion. Once the brain is identified through a connected component operation, a corresponding dilation is applied to reverse the effects of erosion. Finally, BSE uses a morphological closing operation to fill small pits and holes on the brain surface. The method relies on fixed parameters, including diffusion iterations, diffusion constant, edge constant, and erosion size. However, since BSE is edge-based, it can struggle with images that have poor contrast [12].

Supervised approaches also leverage graphs. In [13], a supervised graph-based neural network (GNN) is employed for brain tumor segmentation. The 3D MRI undergoes division into supervoxels using the Simple Linear Iterative Clustering (SLIC) algorithm [14] to prevent the graph from becoming overly complex. SLIC is executed with 15,000 clusters. To mitigate graph and network complexity, the graph is constructed solely with the supervoxels generated by SLIC. Despite showcasing promising results, this method demands several hours for training and relies on labeled data.

SynthStrip [15] is an innovative supervised deep learning method for skull stripping, utilizing a U-Net architecture. Trained on datasets with diverse resolutions and dimensions, it demonstrates superior performance compared to existing methods. However, despite its advancements, there is room for improvement as the method, in certain cases, includes non-brain tissue in the segmentation.

Deep learning methods are increasingly used in various segmentation tasks, showing promising results. The U-Net architecture, in particular, is widely employed for medical image segmentation. In [16], a modified U-Net model is applied to segment newborn brain images by training on 243 adult data and only 5 newborn data. This approach demonstrates good results and is compared to SynthStrip. However, as mentioned in [16], manually labeling a single brain volume takes approximately 8 hours, which is time-consuming for medical staff. For the skull-stripping task, where brain structures are relatively consistent, unsupervised methods, such as the proposed approach, could be a promising alternative.

3. Outlined method

The method described here is founded on the concept presented in [4]. It involves transforming each MRI into a weighted graph, where the voxels in the MRI serve as nodes, and adjacent nodes are connected by edges. The weight of each edge is determined by calculating the absolute difference in intensity between the two connected nodes. Similar to [4], [3], and [5], the segmentation involves the utilization of a Minimum Spanning Tree (MST). In contrast to the approach presented in [5] and akin to the methods

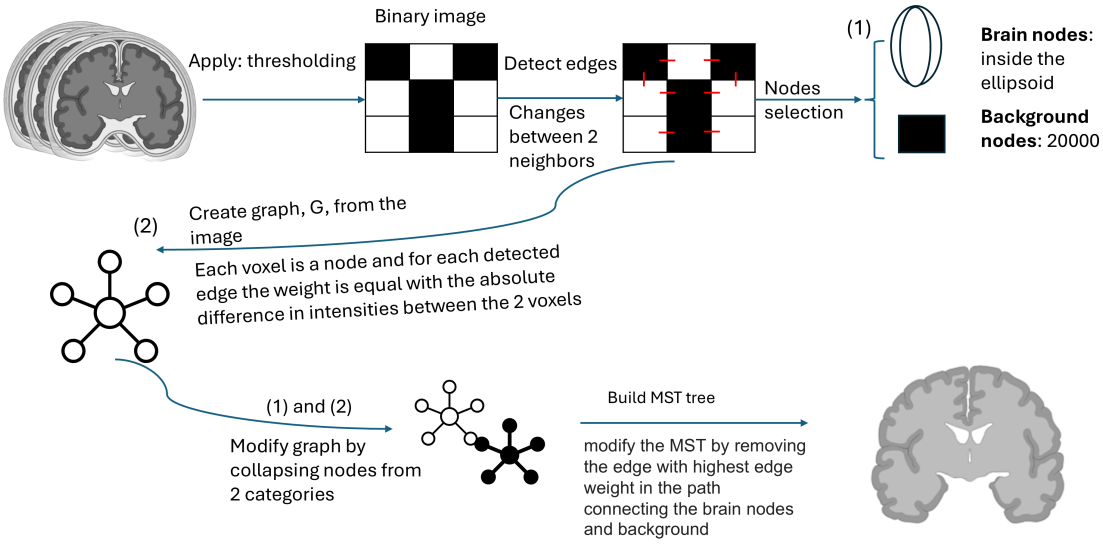

Figure 1: Overview of the main steps of the proposed approach

in [4] and [3], nodes are chosen from two categories—specifically, nodes within the brain and nodes from the background. Nodes within the brain are selected within an ellipsoid, similar to the approach in [4]. The key distinction from [4] lies in the fact that the node selection employs an ellipsoid centered at the center of the image, rather than at the center of mass as proposed in [4]. The method is divided in the following steps, which are also illustrated in Figure 1:

- Image processing
- Nodes sampling
- MST construction & Brain extraction

3.1. Image processing

During the processing phase, a singular operation takes place: applying binary closing to fill gaps, a technique commonly used when sampling nodes in the background. To maintain resolution and details, the images are employed in their original dimensions, preventing any loss.

3.2. Nodes sampling

Constructing a graph involves the creation of nodes and edges. In this scenario, voxels represent the nodes, and an edge is established between every two adjacent nodes. Nodes are selected from two distinct categories: nodes within the brain and nodes in the background. The background nodes follow the methodology outlined in [5]. Initially, a binary image is computed using Otsu thresholding. Subsequently, as described in the processing phase, binary closing is applied. After obtaining the transformed binary image, 20,000 voxels are randomly selected from the six faces.

Sampling nodes from the brain involves constructing an ellipsoid. The inspiration for using an ellipsoid is drawn from [2], where the brain was approximated using this geometric shape. In previous methods, the center of these geometrical bodies was positioned at the center of mass in the image, a concept derived from the BET method. However, in certain images, the center of mass might be located in a corner, leading to the oversight of crucial parts of the brain during node sampling. To address this issue, the proposed approach sets the center of the ellipsoid at the image's center, calculated for

each axis. For an MRI with the dimensions (dim_x, dim_y, dim_z) the center of the image will be located in $(\frac{dim_x}{2}, \frac{dim_y}{2}, \frac{dim_z}{2})$.

For the x, y, and z axes, any nodes that meet the conditions specified in (1), which represents the ellipsoid equation, are identified as nodes within the brain. r is determined by considering the volume of voxels that surpass the multi-Otsu threshold. Increasing the dimensions of the ellipsoid axes results in a growth in the number of the selected nodes, which denotes a more complex graph. On the other hand, reducing the size for the dimensions results in a too small graph.

$$9 \cdot \frac{x^2}{r^2} + 9 \cdot \frac{y^2}{r^2} + \frac{9}{16} \cdot \frac{z^2}{r^2} \leq 1 \tag{1}$$

3.3. MST construction & Brain segmentation

MST construction follows a similar approach as described in [5] and [4]. Constructing the MST involves transforming the initial graph, representing the MRI into a smaller graph that can be processed more easily. Nodes from the two categories are combined into a single representative node. The graph transformation involves collapsing nodes based on the following rules: if two nodes connected by an edge are part of the multitude of sampling nodes, the edge is discarded, and both nodes are replaced by a single representative node for each category. Subsequently, for the remaining edges containing one node from the sampled category, that node is replaced by the single representative node, and all other nodes from the sampled category are removed except for the single representative one.

The segmentation process concludes with a step that divides the image into two regions: the brain and the background. This is accomplished by removing the edge with the highest weight from the Minimum Spanning Tree (MST) path [4].

4. Results

To assess the effectiveness of the proposed method, multiple datasets were utilized. The Neurofeedback Skull-stripped repository (NFBS) comprises 125 T1w MRI images from subjects aged between 21 and 45, representing a diverse range of clinical and subclinical psychiatric conditions. Additionally, a dataset used for testing and validation in [15] consists of 625 images sourced from seven public datasets, each offering distinct modalities and resolutions.

The method was specifically tested on a subset of the [15] dataset, focusing on 48 T1w MRI images from the IXI dataset [1], 36 T2 MRI images from the FSM dataset [17], and 16 infant T1w MRIs from [18]. The choice of datasets and subsets of images adheres to the methodology outlined in [15].

We compared our results to two state-of-the-art methods which are broadly used, BET2 from FSL Tool [9, 19, 20] and the BSE from Brain Suite Tool [21, 22].

4.1. Evaluation metrics

To evaluate the effectiveness of the proposed method, six metrics were employed: accuracy, precision, sensitivity, specificity, Jaccard Index, and Dice Coefficient. These metrics were computed by comparing the predicted MRI images with the ground truth. In this context, TP denotes voxels correctly identified as brain tissue, TN represents voxels inaccurately identified as non-brain tissue, FP indicates voxels mistakenly identified as brain tissue, and FN refers to voxels within the brain region inaccurately identified as non-brain tissue [3].

Voxel accuracy [23, 3] is defined as 2 and denotes the proportion of accurately classified voxels.

$$Accuracy = \frac{TP + TN}{TP + TN + FP + FN} \tag{2}$$

[1] $http://brain-development.org/ixi-dataset/$

Precision [24, 3] is computed with the formula 3 and denotes the percentage of the accurately classified voxels in the brain tissue.

$$Precision = \frac{TP}{TP + FP} \tag{3}$$

Sensitivity [24, 3], calculated as 4 measures the percentage of brain tissue voxels in the ground truth that are accurately detected as brain tissue in the prediction.

$$Sensitivity = \frac{TP}{TP + FN} \tag{4}$$

Specificity [24, 3], determined with 5 represents the ratio of non-brain tissue voxel in the ground truth that are correctly identified as non-brain in the prediction.

$$Specificity = \frac{TN}{TN + FN} \tag{5}$$

Jaccard Index [24, 3], defined as 6 presents the overlap between the ground truth and segmentation results, divided by the union between the ground truth and segmentation results

$$JaccardIndex = \frac{TP}{TP + FP + FN} \tag{6}$$

Dice Coefficient [24, 3], having the formula 7 quantifies the resemblance between the two sets of labels.

$$Dicecoefficient = \frac{2TP}{2TP + FP + FN} \tag{7}$$

4.2. Numerical results

Table 1 provides a comparative analysis of Ellipsoid-GUBS, the newly proposed approach, BET2 and BSE methods on the NFBS [6] dataset. The new proposed approach slightly improved in the Sensitivity with 4% in comparison to Ellipsoid-GUBS. For the NFBS dataset, the new proposed approach shows slight improvements in almost all metrics compared to BET2, with the exception of sensitivity. This means BET2 identifies true positives more effectively than the new approach. However, the new method demonstrates a notable 10% improvement in precision compared to BET2, indicating that it correctly identifies positive cases more accurately. However, BSE demonstrated the best performance.

Table 1
Results on the NFBS Dataset

	Ellipsoid-GUBS	New approach	BET2	BSE
Accuracy	0.9520 ± 0.0237	0.9484 ± 0.0263	0.9322 ± 0.0434	0.9905 ± 0.0195
Precision	0.8218 ± 0.1359	0.7795 ± 0.1388	0.6783 ± 0.1870	0.9483 ± 0.0889
Jaccard	0.6105 ± 0.1529	0.6138 ± 0.0912	0.5979 ± 0.1489	0.9202 ± 0.0872
Dice	0.7437 ± 0.1534	0.7565 ± 0.0748	0.7371 ± 0.1215	0.9545 ± 0.0871
Specificity	0.9781 ± 0.0267	0.9700 ± 0.0309	0.9419 ± 0.0489	0.9937 ± 0.0133
Sensitivity	0.7195 ± 0.1806	0.7557 ± 0.0803	0.8472 ± 0.0541	0.9615 ± 0.0892

Table 2 summarizes the results for infant T1w images from the QIN [25] dataset. The novel approach shows slight improvements in all metrics compared to Ellipsoid-GUBS, including a 3% increase in both the Dice coefficient and Jaccard index. When compared to BET2, the proposed method achieves a 14% increase in precision and a 13% increase in the Jaccard index. Furthermore, it improves sensitivity by 21% and the Dice coefficient by 6% when compared to the BSE method.

Table 3 reports the results of experiments on 48 MRIs from the IXI dataset. All methods yield comparable results, though BET2 achieves slightly better scores overall.

Table 2
Results on the Infant T1w dataset

	Ellipsoid-GUBS	New approach	BET2	BSE
Accuracy	0.9553 ± 0.0625	0.9583 ± 0.0635	0.9438 ± 0.0428	0.9414 ± 0.0942
Precision	0.6038 ± 0.1982	0.6408 ± 0.1849	0.5085 ± 0.1957	0.6566 ± 0.3646
Jaccard	0.6006 ± 0.1946	0.6374 ± 0.1816	0.5075 ± 0.1949	0.6385 ± 0.3540
Dice	0.7306 ± 0.1646	0.7615 ± 0.1548	0.6496 ± 0.1853	0.7031 ± 0.3588
Specificity	0.9530 ± 0.0673	0.9561 ± 0.0683	0.9411 ± 0.0443	0.9504 ± 0.0775
Sensitivity	0.9951 ± 0.0081	0.9948 ± 0.0081	0.9981 ± 0.0036	0.7874 ± 0.3795

Table 3
Results on the IXI T1w dataset

	Ellipsoid-GUBS	New approach	BET2	BSE
Accuracy	0.9294 ± 0.0382	0.9275 ± 0.0379	0.9606 ± 0.0307	0.9672 ± 0.0460
Precision	0.7222 ± 0.1307	0.7128 ± 0.0129	0.8377 ± 0.1179	0.9283 ± 0.1643
Jaccard	0.6807 ± 0.1118	0.6739 ± 0.1105	0.7945 ± 0.1109	0.8426 ± 0.1361
Dice	0.8047 ± 0.0796	0.7999 ± 0.0801	0.8808 ± 0.0760	0.9074 ± 0.0974
Specificity	0.9290 ± 0.0484	0.9263 ± 0.0475	0.9643 ± 0.0351	0.9770 ± 0.0577
Sensitivity	0.9309 ± 0.0455	0.9338 ± 0.4330	0.9393 ± 0.0193	0.9099 ± 0.0294

Table 4
Results on the FMS T2w dataset for the Graph based approach, BET2 and BSE

	Ellipsoid-GUBS	New approach	BET2	BSE
Accuracy	0.9899 ± 0.0017	0.9883 ± 0.0026	0.9836 ± 0.0142	0.8331 ± 0.0503
Precision	0.9734 ± 0.0155	0.9556 ± 0.0251	0.8668 ± 0.0908	0.2019 ± 0.2646
Jaccard	0.8940 ± 0.0139	0.8806 ± 0.0208	0.8564 ± 0.0892	0.1633 ± 0.2038
Dice	0.9439 ± 0.0078	0.9363 ± 0.0119	0.9200 ± 0.0600	0.2337 ± 0.2724
Specificity	0.9973 ± 0.0016	0.9955 ± 0.0028	0.9834 ± 0.01547	0.8841 ± 0.0424
Sensitivity	0.9164 ± 0.0086	0.9179 ± 0.0080	0.9863 ± 0.0060	0.3258 ± 0.3760

Table 4 presents the outcomes for the FMS T2w dataset. The new approach performs similarly to Ellipsoid-GUBS but shows improvements in all metrics compared to both BET2 and BSE.

We conducted the Repeated Measures ANOVA test on the four datasets to evaluate the performance differences among the four methods. The results indicated a significant difference ($p < 0.05$) in most cases, with one exception (Infant dataset). Additionally, a Wilcoxon test revealed that the proposed new approach was significantly different from the BSE method on FSM dataset. However, for the other datasets, the Wilcoxon tests did not show a significant difference for the proposed method, while some differences were significant for the other methods. This lack of significance in the Wilcoxon tests is likely due to the small sample size.

4.3. Visual results

Figure 2 displays the visual results for each dataset. Although the numerical data may not fully highlight the differences, the visual comparison reveals the improvements achieved by the proposed method. For the NFBS dataset, the novel approach is closer to the ground truth than the Ellipsoid-GUBS method, which removed parts of the brain. Also, in the case of the IXI dataset, a considerable part of the skull was removed, which results in an overall better segmentation in comparison to the Ellipsoid-GUBS method. The Infant dataset also shows enhanced segmentation with the new approach, leaving only a small part of the skull. Conversely, for the FMS dataset, the performance of the methods is similar.

The implementation was done in python programming language and the experiments were run on an i7 processor (Core i7-8750HCPU @ 2.2GHz). In terms of experimental timing, it takes almost 45

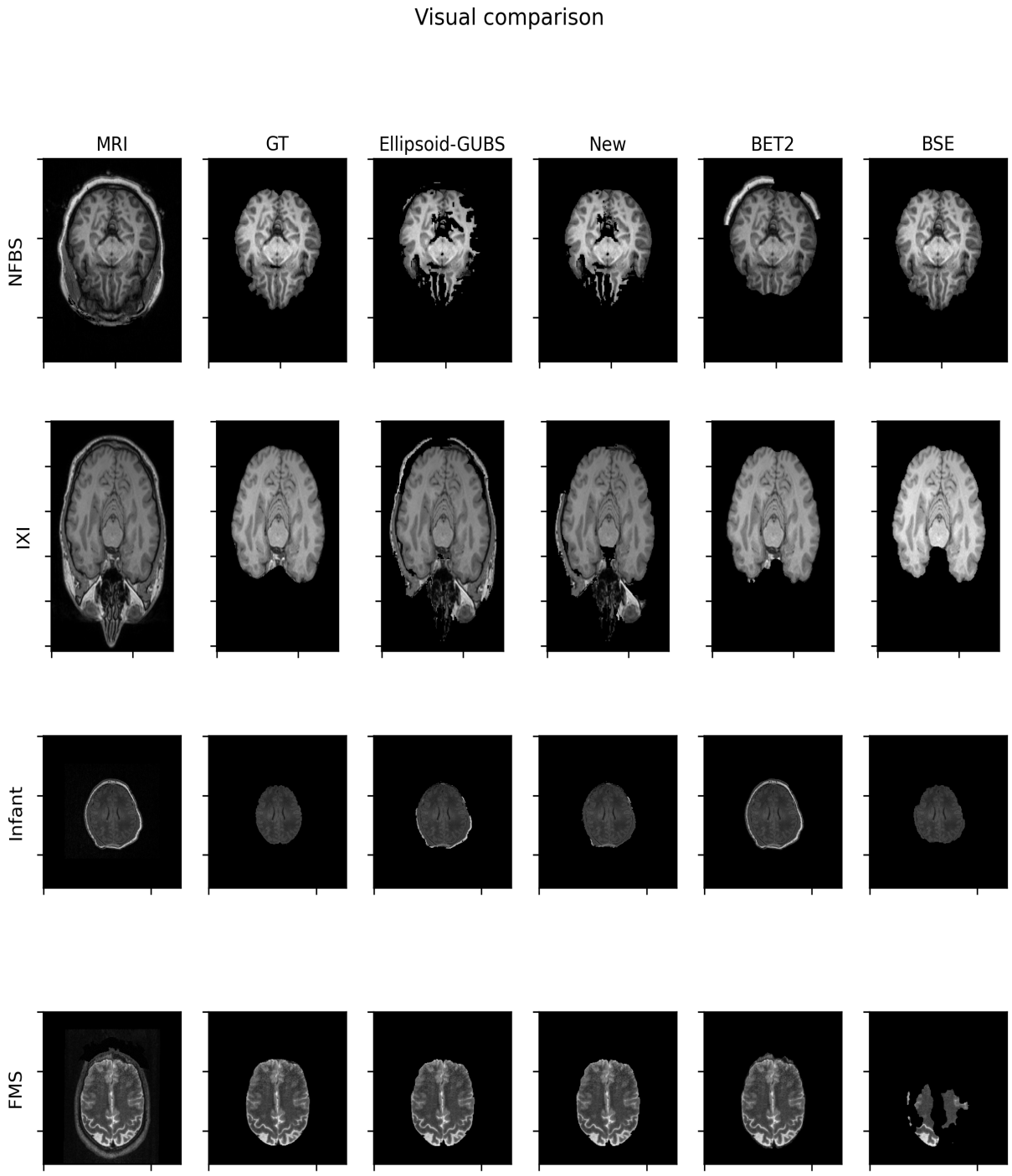

Figure 2: Visual comparison for each dataset used in the evaluation for the axial slice, first column represents the original slice, second the ground truth, third Ellipsoid-GUBS, the fourth the segmentation obtained for the novel proposed approach, the fifth represents the segmentation obtained with BET and the last one with BSE methods

seconds for the algorithm to perform the segmentation using images at their original size.

5. Discussion

The proposed method introduces several key contributions, including a shift to geometric centering for improved stability across datasets and comprehensive validation on four diverse datasets, demonstrating

its robustness. Additionally, the method's benchmarking against two state-of-the-art techniques, BET2 and BSE, highlights its superior performance, particularly with T2-weighted and infant data.

The method presented underwent testing on four diverse datasets with varying resolutions and dimensions. Employing a minimal spanning tree, the novel approach extracted brain structures by constructing a graph from nodes within the brain and the background. Specifically, voxels situated within an ellipsoid centered at the image's geometric center were considered nodes representing the brain. The method was compared to two state-of-the-art techniques, yielding comparable results and even achieving better segmentation on certain datasets.

While acknowledging the advancements achieved by the presented method and its independence from the type of MRI, it is noteworthy that there remains potential for further enhancement. The current results indicate a positive trajectory, yet ongoing refinement is crucial to push the boundaries of segmentation accuracy. Notably, the method stands out for its efficiency and speed, a notable advantage in the context of medical imaging where swift processing is often imperative.

Although the numerical results between the new approach and the two state-of-the-art methods are comparable, the segmentation performance varies across different datasets: For the FMS T2w dataset, BSE failed to segment the brain, whereas the new approach and BET2 performed better, with the new approach achieving the most accurate segmentation. However, BET2 still included some non-brain parts. For the Infant dataset, BET2 was unable to remove the skull, while the new approach and BSE both performed similarly, close to the ground truth. In the IXI dataset, the new approach retained some non-brain parts, while the others successfully removed the skull. On the NFBS dataset, BSE provided the best segmentation, followed by the new approach, whereas BET2 included some skull remnants. Overall, improvements between the Ellipsoid-GUBS and the new approach are evident in all datasets except the FMS dataset, where the results are similar.

6. Conclusions and Future work

The paper introduced an enhanced unsupervised graph-based segmentation method that exhibits improved results across the T1w datasets subjected to testing. When applied to the T2w dataset, the method shows comparable outcomes to the method it was compared against. The segmentation process involves utilizing a Minimum Spanning Tree (MST), and the node selection is performed using an ellipsoid centered within the image.

The proposed method was evaluated against two state-of-the-art methods, BET2 and BSE, and demonstrated superior performance. On the infant dataset, it achieved a 21% increase in sensitivity compared to the BSE method, along with a 14% improvement in precision and a 13% increase in the Jaccard index compared to BET2. On the NFBS dataset, the method showed a 10% improvement in precision over BET2. However, on the T2w dataset, the method provided only slight improvements compared to both BSE and BET2.

Future endeavors encompass expanding the method's evaluation to additional datasets, conducting comparisons with other state-of-the-art and deep learning methods. Additionally, there are plans for collaboration with a hospital to acquire real-world data.

Declaration on Generative AI

During the preparation of this work, the authors used ChatGPT and Grammarly in order to: Grammar and spelling check, Paraphrase and reword. After using this tools, the authors reviewed and edited the content as needed and take full responsibility for the publication's content.

Data availability

The datasets utilized in this study can be accessed from their original websites:

NFBS: http://preprocessed-connectomes-project.org/NFB_skullstripped/

SYNTHSTRIP (which contains the images for the IXI dataset, Infant T1w dataset, FMS T2w dataset): https://surfer.nmr.mgh.harvard.edu/docs/synthstrip/#dataset

References

[1] S. M. Smith, Fast robust automated brain extraction, Hum Brain Mapp 17 (2002) 143–155.

[2] L. Wang, Z. Zeng, R. Zwiggelaar, An improved bet method for brain segmentation, in: 2014 22nd International Conference on Pattern Recognition, 2014, pp. 3221–3226. doi:10.1109/ICPR.2014.555.

[3] M. Popa, An 3d mri unsupervised graph-based skull stripping algorithm, Procedia Computer Science 225 (2023) 1682–1690. URL: https://www.sciencedirect.com/science/article/pii/S1877050923013157. doi:https://doi.org/10.1016/j.procs.2023.10.157, 27th International Conference on Knowledge Based and Intelligent Information and Engineering Sytems (KES 2023).

[4] M. Popa, A. Andreica, Towards an improved unsupervised graph-based mri brain segmentation method, in: M. Sellami, M.-E. Vidal, B. van Dongen, W. Gaaloul, H. Panetto (Eds.), Cooperative Information Systems, Springer Nature Switzerland, Cham, 2024, pp. 480–487.

[5] S. Mayala, I. Herdlevær, J. B. Haugsøen, S. Anandan, N. Blaser, S. Gavasso, M. Brun, Gubs: Graph-based unsupervised brain segmentation in mri images, Journal of Imaging 8 (2022). URL: https://www.mdpi.com/2313-433X/8/10/262. doi:10.3390/jimaging8100262.

[6] B. Puccio, J. P. Pooley, J. S. Pellman, E. C. Taverna, R. C. Craddock, The preprocessed connectomes project repository of manually corrected skull-stripped T1-weighted anatomical MRI data, GigaScience 5 (2016). URL: https://doi.org/10.1186/s13742-016-0150-5. doi:10.1186/s13742-016-0150-5. arXiv:https://academic.oup.com/gigascience/article-pdf/5/1/s13742-016-0150-5/25513149/author_comments-benjamin_puccio_v2.pdf, s13742-016-0150-5.

[7] S. A. Sadananthan, W. Zheng, M. W. Chee, V. Zagorodnov, Skull stripping using graph cuts, NeuroImage 49 (2010) 225–239. URL: https://www.sciencedirect.com/science/article/pii/S1053811909009604. doi:https://doi.org/10.1016/j.neuroimage.2009.08.050.

[8] M. Jenkinson, Bet2: Mr-based estimation of brain, skull and scalp surfaces, in: Eleventh Annual Meeting of the Organization for Human Brain Mapping, 2005, 2005.

[9] M. Jenkinson, C. F. Beckmann, T. E. Behrens, M. W. Woolrich, S. M. Smith, Fsl, NeuroImage 62 (2012) 782–790. URL: https://www.sciencedirect.com/science/article/pii/S1053811911010603. doi:https://doi.org/10.1016/j.neuroimage.2011.09.015, 20 YEARS OF fMRI.

[10] K. Ezhilarasan, S. Praveenkumar, K. Somasundaram, T. Kalaiselvi, S. Magesh, S. Kiruthika, A. Jeevarekha, Automatic brain extraction from mri of human head scans using helmholtz free energy principle and morphological operations, Biomedical Signal Processing and Control 64 (2021) 102270. URL: https://www.sciencedirect.com/science/article/pii/S1746809420303955. doi:https://doi.org/10.1016/j.bspc.2020.102270.

[11] L. Pei, M. Ak, N. H. M. Tahon, S. Zenkin, S. Alkarawi, A. Kamal, M. Yilmaz, L. Chen, M. Er, N. Ak, et al., A general skull stripping of multiparametric brain mris using 3d convolutional neural network, Scientific Reports 12 (2022) 10826.

[12] K. Palanisamy, S. Prasath, Methods on skull stripping of mri head scan images-a review, Journal of Digital Imaging 29 (2015). doi:10.1007/s10278-015-9847-8.

[13] C. Saueressig, A. Berkley, E. Kang, R. Munbodh, R. Singh, Exploring graph-based neural networks for automatic brain tumor segmentation, in: J. Bowles, G. Broccia, M. Nanni (Eds.), From Data to Models and Back, Springer International Publishing, Cham, 2021, pp. 18–37.

[14] R. Achanta, A. Shaji, K. Smith, A. Lucchi, P. Fua, S. Süsstrunk, Slic superpixels compared to state-of-the-art superpixel methods, IEEE Transactions on Pattern Analysis and Machine Intelligence 34 (2012) 2274–2282. doi:10.1109/TPAMI.2012.120.

[15] A. Hoopes, J. S. Mora, A. V. Dalca, B. Fischl, M. Hoffmann, Synthstrip: skull-stripping for any

brain image, NeuroImage 260 (2022) 119474. doi:https://doi.org/10.1016/j.neuroimage.2022.119474.

[16] A. Omidi, A. Mohammadshahi, N. Gianchandani, R. King, L. Leijser, R. Souza, Unsupervised domain adaptation of mri skull-stripping trained on adult data to newborns, in: Proceedings of the IEEE/CVF Winter Conference on Applications of Computer Vision (WACV), 2024, pp. 7718–7727.

[17] D. N. Greve, B. Billot, D. Cordero, A. Hoopes, M. Hoffmann, A. V. Dalca, B. Fischl, J. E. Iglesias, J. C. Augustinack, A deep learning toolbox for automatic segmentation of subcortical limbic structures from mri images, NeuroImage 244 (2021) 118610. doi:https://doi.org/10.1016/j.neuroimage.2021.118610.

[18] K. de Macedo Rodrigues, E. Ben-Avi, D. D. Sliva, M.-s. Choe, M. Drottar, R. Wang, B. Fischl, P. E. Grant, L. Zöllei, A freesurfer-compliant consistent manual segmentation of infant brains spanning the 0-2 year age range, Frontiers in Human Neuroscience 9 (2015). URL: https://www.frontiersin.org/articles/10.3389/fnhum.2015.00021. doi:10.3389/fnhum.2015.00021.

[19] S. M. Smith, M. Jenkinson, M. W. Woolrich, C. F. Beckmann, T. E. Behrens, H. Johansen-Berg, P. R. Bannister, M. De Luca, I. Drobnjak, D. E. Flitney, R. K. Niazy, J. Saunders, J. Vickers, Y. Zhang, N. De Stefano, J. M. Brady, P. M. Matthews, Advances in functional and structural mr image analysis and implementation as fsl, NeuroImage 23 (2004) S208–S219. URL: https://www.sciencedirect.com/science/article/pii/S1053811904003933. doi:https://doi.org/10.1016/j.neuroimage.2004.07.051, mathematics in Brain Imaging.

[20] M. W. Woolrich, S. Jbabdi, B. Patenaude, M. Chappell, S. Makni, T. Behrens, C. Beckmann, M. Jenkinson, S. M. Smith, Bayesian analysis of neuroimaging data in fsl, NeuroImage 45 (2009) S173–S186. URL: https://www.sciencedirect.com/science/article/pii/S1053811908012044. doi:https://doi.org/10.1016/j.neuroimage.2008.10.055, mathematics in Brain Imaging.

[21] S. Sandor, R. Leahy, Surface-based labeling of cortical anatomy using a deformable atlas, IEEE Transactions on Medical Imaging 16 (1997) 41–54. doi:10.1109/42.552054.

[22] D. W. Shattuck, R. M. Leahy, Brainsuite: An automated cortical surface identification tool, Medical Image Analysis 6 (2002) 129–142. URL: https://www.sciencedirect.com/science/article/pii/S1361841502000543. doi:https://doi.org/10.1016/S1361-8415(02)00054-3.

[23] H. Zhang, J. E. Fritts, S. A. Goldman, Image segmentation evaluation: A survey of unsupervised methods, Computer Vision and Image Understanding 110 (2008) 260–280. URL: https://www.sciencedirect.com/science/article/pii/S1077314207001294. doi:https://doi.org/10.1016/j.cviu.2007.08.003.

[24] A. A. Taha, A. Hanbury, Metrics for evaluating 3d medical image segmentation: analysis, selection, and tool, BMC Medical Imaging 15 (2015).

[25] K. Clark, B. Vendt, K. Smith, J. Freymann, J. Kirby, P. Koppel, S. Moore, S. Phillips, D. Maffitt, M. Pringle, L. Tarbox, F. Prior, The cancer imaging archive (tcia): Maintaining and operating a public information repository, Journal of digital imaging 26 (2013). doi:10.1007/s10278-013-9622-7.